π-Topology and Spin Alignment Utilizing the Excited Molecular Field: Observation of the Excited High-Spin Quartet ($S = 3/2$) and Quintet ($S = 2$) States on Purely Organic π-Conjugated Spin Systems

Yoshio Teki,*,†,‡ Sadaharu Miyamoto,‡ Masaaki Nakatsuji,§ and Yozo Miura§

Contribution from Structure and Transformation, PRESTO JST, the Department of Material Science, Graduate School of Science, and the Department of Applied Chemistry, Faculty of Engineering, Osaka City University, 3-3-138 Sugimoto, Sumiyoshi-ku, Osaka 558-8585, Japan

Received May 31, 2000. Revised Manuscript Received October 6, 2000

Abstract: As a model system for the photoinduced/photoswitched spin alignment in a purely organic *π-conjugated* spin system, 9-[4-(4,4,5,5-tetramethyl-1-yloxyimidazolin-2-yl)phenyl]anthracene (**1a**), 9-[3-(4,4,5,5-tetramethyl-1-yloxyimidazolin-2-yl)phenyl]anthracene (**1b**), 9,10-bis[4-(4,4,5,5-tetramethyl-1-yloxyimidazolin-2-yl)phenyl]anthracene (**2a**), and 9,10-bis[3-(4,4,5,5-tetramethyl-1-yloxyimidazolin-2-yl)phenyl]anthracene (**2b**) were designed and synthesized. In these spin systems, 9-phenylanthracene and 9,10-diphenylanthracene were chosen as photo spin couplers and iminonitroxide was chosen as a dangling stable radical. Time-resolved electron spin resonance (TRESR) spectra of the first excited states with resolved fine-structure splittings were observed for **1a** and **2a** in an EPA or a 2-MTHF rigid glass matrix. Using the spectral simulation based on the eigenfield method, the observed TRESR spectra for **1a** and **2a** were unambiguously assigned as an excited quartet ($S = 3/2$) spin state (Q) and an excited quintet ($S = 2$) spin state (Qu), respectively. The g value and fine-structure splitting for the quartet state of **1a** were determined to be $g(\mathrm{Q}) = 2.0043$, $D(\mathrm{Q}) = 0.0235\ \mathrm{cm}^{-1}$, and $E(\mathrm{Q}) = 0.0\ \mathrm{cm}^{-1}$. The relative populations (polarization) of each M_S sublevel in Q were determined to be $P_{+1/2'} = P_{-1/2'} = 0.5$ and $P_{+3/2'} = P_{-3/2'} = 0.0$ with an increasing order of energy in zero magnetic field. The spin Hamiltonian parameters for Qu are $g = 2.0043$, $D = 0.0130\ \mathrm{cm}^{-1}$, and $E = 0.0\ \mathrm{cm}^{-1}$, and the relative populations in Qu were determined to be $P_{0'} = 0.30$, $P_{-1'} = P_{+1'} = 0.35$ and $P_{-2'} = P_{+2'} = 0.0$. These are the first observations of a photoexcited quartet and a quintet high-spin state in π-conjugated triplet−radical pair systems. In contrast high-spin excited states were not observed for **1b** and **2b**, the π-topological isomers of **1a** and **2a**, showing the role of π-topology in the spin alignment of the excited states. Since a weak antiferromagnetic exchange interaction was observed in the ground state of **2a**, the clear detection of the excited quintet high-spin state shows that the effective exchange coupling between the two dangling radicals through the diphenylanthracene spin coupler has been changed from antiferromagnetic to ferromagnetic upon photoexcitation. Thus, a photoinduced spin alignment utilizing the excited triplet molecular field was realized for the first time in the purely organic π-conjugated spin system. Furthermore, the mechanism for the generation of dynamic electron spin polarization was investigated for the observed quartet and quintet states, and a plausible mechanism of the enhanced selective intersystem crossing was proposed. Ab initio molecular orbital calculations based on density functional theory were carried out to determine the electronic structures of the excited high-spin states and to understand the mechanism of the spin alignment utilizing the excited molecular field. The role of the spin delocalization and the spin polarization mechanisms were revealed on the photoexcited state.

1. Introduction

Intramolecular spin alignment and exchange interactions through π-conjugation in purely organic spin systems are quite important in the field of molecule-based magnetism.[1] However, most studies are limited to ground-state systems. The studies of the spin alignment between stable radicals and a metastable excited triplet state will give very important information on the novel spin alignment, and could lead to a new strategy for photoinduced/photoswitching magnetic spin systems. In a previous paper,[2] we reported the first observation of a purely organic excited quartet ($S = 3/2$) state and a quintet ($S = 2$) state in *π-conjugated spin systems* which were generated by a spin alignment through π-conjugation between dangling stable iminonitroxide radicals ($S = 1/2$) and the excited triplet ($S = 1$) state of a phenyl- or diphenylanthracene derivative.

Recently, radical (R)−excited triplet (T) pairs in solution have been extensively investigated by the time-resolved electron spin

† Structure and Transformation.
‡ Department of Material Science.
§ Department of Applied Chemistry.

(1) (a) Miller, J. S., Dougherty, D. A., Eds. *Mol. Cryst. Liq. Cryst. 305/306*, Proceedings of the Symposium on Ferromagnetic and High-Spin Molecular Materials, 197th National Meeting of American Chemical Society, Dallas, TX, Fall 1989. (b) Iwamura, H., Miller J. S., Eds. *Mol. Cryst. Liq. Cryst. 232/233*, Proceedings of the Symposium on the Chemistry and Physics of Molecular-based Magnets, Tokyo, Oct 25−30, 1993. (c) Miller, J. S., Epstein, A. J., Eds. *Mol. Cryst. Liq. Cryst. 271/274*, Proceedings of the IVth International Conference on Molecule-based Magnets, Salt Lake City, UT, Oct 16−21, 1995. (d) Itoh, K., Miller, J. S., Takui, T., Eds. *Mol. Cryst. Liq. Cryst. 305/306*, Proceedings of the Vth International Conference on Molecule-based Magnets, Osaka, July 15−20, 1996. (e) Kahn, O., Ed. *Mol. Cryst. Liq. Cryst. 334/ 335*, Proceedings of the VIth International Conference on Molecule-based Magnets, Seignosse, Sept 12−17, 1998.

10.1021/ja001920k CCC: $20.00
Published on Web 12/16/2000

resonance (TRESR) technique,[3] and the contribution of the high-spin quartet state to the chemically induced dynamic electron polarization (CIDEP) mechanism has been pointed out.[4−6] However, only a few examples involving the direct observation of an excited high-spin states ($S \geq 3/2$) generated from a radical−excited triplet pair have been reported. The first direct TRESR detection of an excited quartet state of a radical−excited triplet pair was reported for a fullerene−mononitroxide radical system in solution by Corvaja et al.[7a] and for a tetraphenylporphilinatozinc(II) (ZnTPP) coordinated by *p*-pyridyl nitronylnitroxide (nitpy) in the solid phase by Yamauchi et al.[8] For homologous systems,[7b,c,8b,9] several excited quartet states have been reported since their pioneering works. For the fullerene−dinitroxide system an excited quintet state was also very recently reported.[10] In these systems, a stable radical couples weakly with the triplet excited chromophore through *σ*-bonds or coordination. On the other hand in our phenylanthracene−iminonitoroxide systems, the stable radicals couple with the phenyl- or diphenylanthracene spin coupler through *π-conjugation*, making a strong exchange interaction possible. Furthermore, as shown in this paper, the topology of the *π*-electron network is important in determining the sign of the exchange interaction and in the molecular design of the photoexcited states on the *π*-conjugated spin systems.

We have prepared 9-[4-(4,4,5,5-tetramethyl-1-yloxyimidazolin-2-yl)phenyl]anthracene (**1a**), 9-[3-(4,4,5,5-tetramethyl-1-yloxyimidazolin-2-yl)phenyl]anthracene (**1b**), 9,10-bis[4-(4,4,5,5-tetramethyl-1-yloxyimidazolin-2-yl)phenyl]anthracene (**2a**), and 9,10-bis[3-(4,4,5,5-tetramethyl-1-yloxyimidazolin-2-yl)phenyl]-anthracene (**2b**) in which 9-phenylanthracene and 9,10-diphenylanthracene were chosen as the spin couplers and the iminonitroxide was chosen as the dangling stable radical. Their molecular structures are shown in Figure 1. In **1a** and **2a**, the stable radicals couple strongly with the excited triplet state of the phenyl- or diphenylanthracene moiety upon photoexcitation, and their triplet moieties are expected to be a suitable photocoupler, causing a ferromagnetic exchange interaction. This leads to the excited quartet ($S = 3/2$) state for **1a** and the excited quintet ($S = 2$) state for **2a**. On the other hand, for **1b** and **2b,** topological isomers of **1a** and **2a**, respectively, such a high-spin state cannot be expected on the basis of the *π*-topological rule established for the organic high-spin molecules.[11−15] In this paper we describe the photoexcited quartet state of **1a** and the photoexcited quintet state of **2a**, detected by TRESR, together with the results of the TRESR experiments for **1b** and **2b**. Furthermore, the relationship between the spin alignment in the excited states and topology on the *π*-electron networks is discussed, and ab initio molecular orbital calculations for the excited spin couplers were performed to clarify the mechanism of the intramolecular spin alignment.

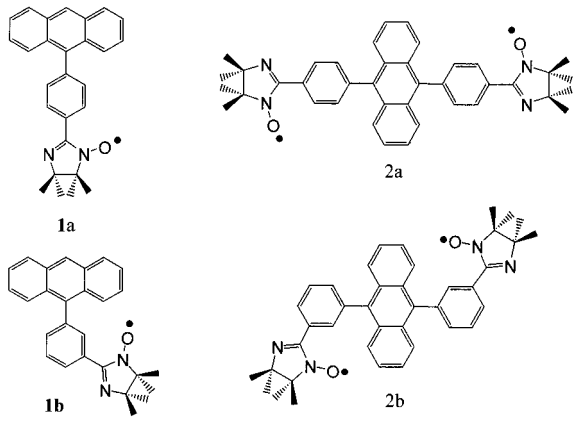

Figure 1. Molecular structure of the phenylanthracene−iminonitroxide and diphenylanthracene−bis(iminonitroxide) compounds studied in this work.

2. Experimental Section

2.1. TRESR Measurement. The TRESR method[3] utilizing CIDEP has been widely used in the study of chemical reactions and short-lived excited states. A conventional X-band ESR spectrometer (JEOL TE300) was used without field modulation in measurements of the TRESR spectra. TRESR signals were amplified by a wide-band preamplifier, transferred to a high-speed digital oscilloscope (LeCroy 9350C) and accumulated, typically, 400 times for each point. Excitation of **1** and **2** was carried out at 355 nm light using a YAG laser (Continuum Surelite II-10). The typical laser power used in the experiments was ca. 5−10 mJ. The temperature was controlled using an Oxford ESR 910 cold He gas flow system. All TRESR experiments were carried out using an EPA or 2-MTHF rigid glass matrix. The glass solvents of the highest commercially available purity were purified by the usual procedure. Samples were degassed by repeated freeze−pump−thaw cycles using a high vacuum line system. TRESR measurements were carried out at 20−40 K.

2.2. Optical Spectrum Measurements and General Method. UV−vis absorption spectra were measured using a HITACHI U-3000 absorption spectrometer at room temperature. Fluorescence emission spectra were obtained at liquid N_2 temperature with a HITACHI F-4500T spectrometer using a quartz Dewar with rectangular suprazil quartz windows. Melting points were recorded on a Yanagimoto micro melting point apparatus and are uncorrected. IR spectra were obtained on a JASCO FT/IR-230 spectrophotometer. ^{1}H NMR spectra were measured with a JEOL α-400 (400 MHz) or Varian *λ*-300 (300 MHz) spectrometer, and the chemical shifts are expressed in parts per million (δ) using Me_4Si as an internal standard.

(2) Teki, Y.; Miyamoto, S.; Iimura, K.; Nakatsuji, M.; Miura, Y. *J. Am. Chem. Soc*. **2000**, *122*, 984.
(3) Kim, S. S.; Weissman, S. I. *J. Magn. Reson*. **1976**, *24*, 167.
(4) Imamura, T.; Onitsuka, O.; Obi, K. *J. Phys. Chem*. **1986**, *90*, 6471.
(5) Blätter, C.; Paul, J. F. *Chem. Phys. Lett*. **1990**, *166*, 375
(6) Kobori, Y.; Mitsui, M.; Kawai, A.; Obi, K. *Chem. Phys. Lett*. **1996**, *252*, 355 and references therein.
(7) (a) Corvaja, C.; Maggini, M.; Prato, M.; Scorrano, G.; Venzin, M. *J. Am. Chem. Soc*. **1995**, *117*, 8857. (b) Corvaja, C.; Maggini, M.; Ruzzi, M.; Scorrano, G.; Toffoletti, A. *Appl. Magn. Reson.* **1997**, *12*, 477. (c) Mizouchi, N.; Ohba, Y.; Yamauchi, S. *J. Chem. Phys.* **1997**, *101*, 5966. (d) Ceroni, P.; Conti, F.; Corvaja, C.; Maggini, M.; Paolucci, F.; Roffia, S.; Scorrano, G.; Toffoletti, A. *J. Phys. Chem. A* **2000**, *104*, 156.
(8) (a) Ishii, K.; Fujiwara, J.; Ohba, Y.; Yamauchi, S. *J. Am. Chem. Soc*. **1996**, *118*, 13079. (b) Ishii, K.; Fujisawa, J.; Adachi, A.; Yamauchi, S.; Kobayashi, N. *J. Am. Chem. Soc*. **1998**, *120*, 3152.
(9) (a) Ishii, K.; Hirose, Y.; Kobayashi, N. *J. Am. Chem. Soc*. **1998**, *120*, 10551. (b) Ishii, K.; Hirose, Y.; Kobayashi, N. *J. Phys. Chem*. **1999**, *103*, 1986.
(10) (a) Mizouchi, N.; Ohba, Y.; Yamauchi, S. *J. Phys. Chem.* **1999**, *103*, 7749. (b) Conti, F.; Corvaja, C.; Toffoletti, A.; Mizouchi, N.; Ohba, Y.; Yamauchi, S.; Maggini, M. *J. Phys. Chem.* **2000**, *104*, 4962. During the review period of our previous paper[2] about the excited quartet and quintet states, the first excited quintet state of a fullerene nitroxide derivative[10a] was reported.
(11) (a) Longuett-Higgins, H. C. *J. Chem. Phys.* **1950**, *18*, 265. (b) Mataga, N. *Theor. Chim. Acta* **1968**, *10*, 372.
(12) (a) Itoh, K. *Chem. Phys. Lett*. **1967**, *1*, 235. (b) Wasserman, E.; Murray, R. W.; Yager W. A.; Trozzolo, A. M.; Smilinsky, G. *J. Am. Chem. Soc*. **1967**, *89*, 5076. (c) Itoh, K. *Pure Appl. Chem*. **1978**, *50*, 1251. (d) Teki, Y.; Takui, T.; Itoh, K.; Iwamura, H.; Kobayashi, K. *J. Am. Chem. Soc*. **1986**, *108*, 2147. (e) Teki, Y.; Itoh, K. In *Magnetic Properties of Organic Materials*; Lahti, P. M., Ed.; Marcel-Dekker: New York, **1999**; pp 237−265 and references therein.
(13) Berson, J. A. In *Magnetic Properties of Organic Materials*; Lahti, P. M., Ed.; Marcel-Dekker: New York, 1999; pp 7−26 and references therein.
(14) (a) Ovchinnikov, A. A. *Theor. Chim. Acta* **1978**, *47*, 297. (b) Klein, D. J.; Nelin, C. J.; Alexander, S.; Matsen, A. *J. Chem. Phys*. **1982**, *77*, 3101.
(15) Borden W. T.; Davidson, E. R. *J. Am. Chem. Soc*. **1977**, *99*, 4587.

Scheme 1

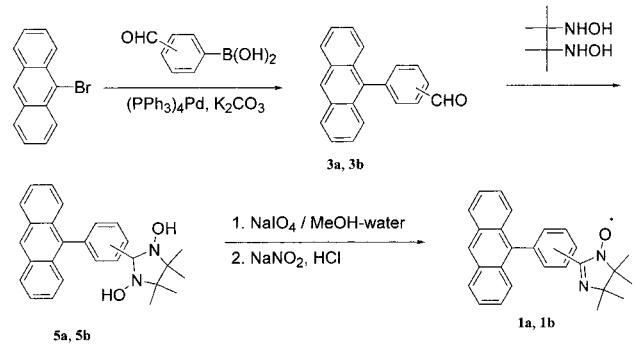

Scheme 2

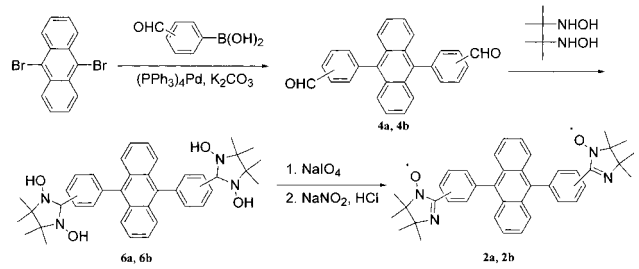

2.3. Materials. 2,3-Bis(hydroxyamino)-2,3-dimethylbutane was prepared according to the literature method.[16] Other reagents were used as purchased. Column chromatography was performed using Fuji Silysia BW-127ZH silica gel (Fuji-Davison Chemical Co., Ltd.). The stable radicals **1** and **2** were synthesized according to the procedures shown in Schemes 1 and 2, respectively.

9-(4-Formylphenyl)anthracene (3a). A mixture of 5.14 g (20 mmol) of 9-bromoanthracene, 3.90 g (26 mmol) of 4-formylphenylboronic acid, 0.69 g (0.60 mmol) of $(PPh_3)_4Pd$, and 11 g of K_2CO_3 in benzene (120 mL)−EtOH (20 mL)−H_2O (40 mL) was refluxed for 24 h under nitrogen.[17] After 50 mL of benzene was added, the organic layer was extracted, washed with brine, and dried with $MgSO_4$. Evaporation, column chromatography (silica gel, benzene), and crystallization (EtOH) gave **3a** in 73% yield (4.12 g, 1.46 mmol) as slightly yellow prisms: mp 144−146 °C; IR (KBr) 1710 cm^{-1} (CHO); ^1H NMR ($CDCl_3$) δ 7.35−7.64 (8H, m, ArH), 8.10−8.12 (4H, m, ArH), 8.54 (1H, s, ArH), 10.19 (1H, s, CHO). Anal. Calcd for $C_{21}H_{14}O$: C, 89.33; H, 5.00. Found: C, 89.07; H, 4.98.

9-(3-Formylphenyl)anthracene (3b). A mixture of 1.03 g (4.0 mmol) of 9-bromoanthracene, 0.78 g (5.2 mmol) of 3-formylphenylboronic acid, 0.14 g (0.12 mmol) of $(PPh_3)_4Pd$, and 2.2 g of K_2CO_3 in benzene (30 mL)−EtOH (6 mL)−H_2O (12 mL) was refluxed for 24 h under nitrogen.[17] After 30 mL of benzene was added, the organic layer was extracted, washed with brine, and dried ($MgSO_4$). Evaporation, column chromatography (silica gel, CH_2Cl_2), and crystallization (EtOH) gave **3b** in 72.6% yield (0.82 g, 2.90 mmol) as yellow prisms: mp 120−122 °C; IR (KBr) 1700 cm^{-1} (CHO); ^1H NMR ($CDCl_3$) δ 7.37 (2H, t, J = 8.0 Hz, ArH), 7.48 (2H, t, J = 8.0 Hz, ArH), 7.56 (2H, d, J = 8.8 Hz, ArH), 7.72 (1H, d, J = 7.8 Hz, ArH), 7.77 (1H, t, J = 7.8 Hz, ArH), 7.96 (1H, s, ArH), 8.07 (2H, d, J = 8.8 Hz, ArH), 8.08 (1H, d, J = 7.8 Hz, ArH), 8.55 (1H, s, ArH), 10.12 (1H, s, CHO). Anal. Calcd for $C_{21}H_{14}O$: C, 89.33; H, 5.00. Found: C, 88.86; H, 4.99.

9,10-Bis(4-formylphenyl)anthracene (4a). A mixture of 5.04 g (15 mmol) of 9,10-dibromoanthracene, 6.0 g (40 mmol) of 4-formylphenylboronic acid, 1.31 g (1.20 mmol) of $(PPh_3)_4Pd$, and 16.69 g of K_2CO_3 in benzene (200 mL)−EtOH (40 mL)−H_2O (80 mL) was refluxed for 48 h under nitrogen and cooled to room temperature.[17] The powder deposited was collected by filtration and washed with water (50 mL) and EtOH (50 mL). Recrystallization from EtOH−benzene gave **4a** in 78% yield (4.52 g, 11.70 mmol) as slightly yellow prisms: mp > 300 °C; IR (KBr) 1710 cm^{-1} (CHO); ^1H NMR ($CDCl_3$) δ 7.36−7.40 (4H, m, ArH), 7.61−7.64 (4H, m, ArH), 7.68 (4H, d, J = 7.8 Hz, ArH), 8.15 (4H, d, J = 7.8 Hz, ArH), 10.21 (2H, s, CHO). Anal. Calcd for $C_{28}H_{18}O_2$: C, 87.02; H, 4.69. Found: C, 86.79; H, 4.60.

9,10-Bis(3-formylphenyl)anthracene (4b). A mixture of 1.35 g (4.0 mmol) of 9,10-dibromoanthracene, 1.56 g (10.4 mmol) of 3-formylphenylboronic acid, 0.29 g (0.25 mmol) of $(PPh_3)_4Pd$, and 4.4 g of K_2CO_3 in benzene (60 mL)−EtOH (12 mL)−H_2O (24 mL) was refluxed for 24 h under nitrogen.[17] After 50 mL of benzene was added, the organic layer was extracted, washed with brine, and dried ($MgSO_4$). Evaporation, column chromatography (silica gel, CH_2Cl_2), and crystallization (EtOH) gave **4b** in 86.8% yield (1.34 g, 3.47 mmol) as slightly yellow prisms: mp > 300 °C; IR (KBr) 1710 cm^{-1} (CHO); ^1H NMR ($CDCl_3$) δ 7.37−7.39 (4H, m ArH), 7.60−7.63 (4H, m, ArH), 7.78−7.83 (4H, m, ArH), 8.02 (2H, d, J = 1.5 Hz, ArH), 8.12 (2H, dd, J = 1.5, 8.8 Hz, ArH), 10.16 (2H, s, CHO). Anal. Calcd for $C_{28}H_{18}O_2$: C, 87.03; H, 4.69. Found: C, 86.82; H, 4.75.

9-[4-(4,4,5,5-Tetramethyl-1,3-dihydroxyimidazolidin-2-yl)phenyl]-anthracene (5a). A mixture of 0.71 g (2.5 mmol) of **4a**, 0.74 g (5.0 mmol) of 2,3-bis(hydroxyamino)-2,3-dimethylbutane, and 0.070 g (0.28 mmol) of 2,3-bis(hydroxyamino)-2,3-dimethylbutane dihydrogen sulfate in MeOH (20 mL)−THF (20 mL) was stirred for 72 h. After evaporation under reduced pressure, 5 mL of MeOH was added, and then 20 mL of H_2O was added to the resulting homogeneous solution. The deposited powder was collected by filtration, washed with H_2O (20 mL) and MeOH (10 mL), and dried in vacuo to give **5a** as a slightly yellow powder in 64% yield (0.66 g, 1.6 mmol).

9-[3-(4,4,5,5-Tetramethyl-1,3-dihydroxyimidazolidin-2-yl)phenyl]-anthracene (5b). A mixture of 0.71 g (2.5 mmol) of **4b**, 0.74 g (5.0 mmol) of 2,3-bis(hydroxyamino)-2,3-dimethylbutane, and 0.070 g (0.28 mmol) of 2,3-bis(hydroxyamino)-2,3-dimethylbutane dihydrogen sulfate in MeOH (20 mL)−THF (20 mL) was stirred for 72 h. After evaporation under reduced pressure, 5 mL of MeOH was added, and then 20 mL of H_2O was added to the resulting homogeneous solution. The deposited powder was collected by filtration, washed with H_2O (20 mL) and MeOH (10 mL), and dried in vacuo to give **5b** as a slightly yellow powder in 51% yield (0.54 g, 1.3 mmol).

9,10-Bis[4-(4,4,5,5-tetramethyl-1,3-dihydroxyimidazolidin-2-yl)-phenyl]anthracene (6a). A mixture of 0.48 g (1.25 mmol) of **5a**, 0.74 g (5.0 mmol) of 2,3-bis(hydroxyamino)-2,3-dimethylbutane, and 0.070 g (0.28 mmol) of 2,3-bis(hydroxyamino)-2,3-dimethylbutane dihydrogen sulfate in MeOH (20 mL)−$CHCl_3$ (20 mL) was refluxed for 72 h. After evaporation under reduced pressure, 5 mL of MeOH was added, and then 20 mL of H_2O was added to the resulting homogeneous solution. The deposited powder was collected by filtration, washed with H_2O (20 mL) and MeOH (10 mL), and dried in vacuo to give **6a** as a slightly yellow powder in 44% yield (1.04 g, 0.55 mmol).

9,10-Bis[3-(4,4,5,5-tetramethyl-1,3-dihydroxyimidazolidin-2-yl)-phenyl]anthracene (6b). A mixture of 0.48 g (1.25 mmol) of **5b**, 0.74 g (5.0 mmol) of 2,3-bis(hydroxyamino)-2,3-dimethylbutane, and 0.070 g (0.28 mmol) of 2,3-bis(hydroxyamino)-2,3-dimethylbutane dihydrogen sulfate in MeOH (20 mL)−$CHCl_3$ (20 mL) was refluxed for 72 h. After evaporation under reduced pressure, 5 mL of MeOH was added, and then 20 mL of H_2O was added to the resulting homogeneous solution. The deposited powder was collected by filtration, washed with H_2O (20 mL) and MeOH (10 mL), and dried in vacuo to give **6b** as a slightly yellow powder in 49% yield (1.04 g, 1.61 mmol).

9-[4-(4,4,5,5-Tetramethyl-1-yloxyimidazolin-2-yl)phenyl]anthracene (1a). To a suspension of 3.17 g (7.68 mmol) of **5a** in 80 mL of benzene was added a solution of 4.71 g (22 mmol) of $NaIO_4$ in 80 mL of H_2O, and the mixture was stirred for 2 h. The organic layer (dark blue) was separated, washed with brine, dried ($MgSO_4$), and evaporated. After 60 mL of CH_2Cl_2 and 9.94 g (0.14 mmol) of $NaNO_2$ in CH_2Cl_2 (20 mL)−H_2O (20 mL) were added to the residue, 1 N HCl was added dropwise to the mixture cooled to 0 °C until the organic layer turned orange.[18] The CH_2Cl_2 layer was then separated, washed with brine, dried ($MgSO_4$), evaporated, and column chromatographed (silica gel,

(16) Lamchen, M.; Mittag, T. W. *J. Chem. Soc. C* **1966**, *2*, 300.
(17) Miyaura, N.; Suzuki, A. *Chem. Rev.* **1995**, *95*, 2457.
(18) (a) Ullman E. F.; Call L.; Osiecki, J. H. *J. Org. Chem.* **1970**, *35*, 3623. (b) Ullman E. F.; Osiecki, J. H.; Boocock, D. G. B.; Darcy, R. *J. Am. Chem. Soc.* **1972**, *94*, 7079. (c) Gatteschi, D.; Rey, P. In *Magnetic Properties of Organic Materials*; Lahti, P. M., Ed.; Marcel-Dekker: New York, 1999; pp 601−627.

CH_2Cl_2), and recrystallization from EtOH gave **1a** in 26.5% yield (0.8 g, 2.03 mmol) as red prisms: mp 190−193 °C; IR (KBr) 3050, 2980, 1610, 1440, 1440, 1360, 1290, 1160, 890, 850, 740 cm^{-1}. Anal. Calcd for $C_{27}H_{25}N_2O$: C, 82.41; H, 6.40; N, 7.12. Found: C, 82.17; H, 6.46, N; 7.01.

9-[3-(4,4,5,5-Tetramethyl-1-yloxyimidazolin-2-yl)phenyl]anthracene (1b). To a suspension of 0.63 g (1.53 mmol) of **5b** in 20 mL of benzene was added a solution of 0.83 g (3.90 mmol) of $NaIO_4$ in 20 mL of H_2O, and the mixture was stirred for 2 h. The organic layer (dark blue) was separated, washed with brine, dried ($MgSO_4$), and evaporated. After 20 mL of CH_2Cl_2 and 2.50 g (36.23 mmol) of $NaNO_2$ in H_2O (20 mL) were added to the residue, 1 N HCl was added dropwise to the mixture cooled to 0 °C until the organic layer turned orange.[18] The CH_2Cl_2 layer was then separated, washed with brine, dried ($MgSO_4$), evaporated, and column chromatographed (silica gel, CH_2Cl_2), and recrystallization from EtOH gave **1b** in 65.0% yield (0.39 g, 1.0 mmol) as red prisms: mp >300 °C; IR (KBr) 2980, 2920, 1610, 1440, 1020, 940, 830, 770, 660, 420 cm^{-1}. Anal. Calcd for $C_{27}H_{25}N_2O$: C, 82.41; H, 6.40; N, 7.12. Found: C, 82.21; H, 6.29, N; 7.09.

9,10-Bis[4-(4,4,5,5-tetramethyl-1-yloxyimidazolin-2-yl)phenyl]anthracene (2a). To a suspension of 1.04 g (1.61 mmol) of **6a** in 30 mL of benzene was added a solution of 1.00 g (4.70 mmol) of $NaIO_4$ in 60 mL of H_2O, and the mixture was stirred for 2 h. The organic layer (dark blue) was separated, washed with brine, dried ($MgSO_4$), and evaporated. After 20 mL of CH_2Cl_2 and 1.10 g (1.59 mmol) of $NaNO_2$ in H_2O (20 mL) were added to the residue, 1 N HCl was added dropwise to the mixture cooled to 0 °C until the organic layer turned orange.[18] The CH_2Cl_2 layer was then separated, washed with brine, dried ($MgSO_4$), evaporated, and column chromatographed (silica gel, CH_2Cl_2), and recrystallization from EtOH gave **2a** in 5.6% yield (60 mg, 0.102 mmol) as red prisms: mp >300 °C; IR (KBr) 2980, 2920, 1540, 1480, 1380, 1300, 1140, 780, 700, 680, 420 cm^{-1}. Anal. Calcd for $C_{40}H_{40}N_4O_2 \cdot H_2O$: C, 76.65; H, 6.75; N, 8.94. Found: C, 76.65; H, 6.63, N; 8.73.

9,10-Bis[3-(4,4,5,5-tetramethyl-1-yloxyimidazolin-2-yl)phenyl]anthracene (2b). To a suspension of 1.04 g (1.61 mmol) of **6b** in 30 mL of benzene was added a solution of 1.00 g (4.70 mmol) of $NaIO_4$ in 60 mL of H_2O, and the mixture was stirred for 2 h. The organic layer (dark blue) was separated, washed with brine, dried ($MgSO_4$), and evaporated. After 20 mL of CH_2Cl_2 and 1.10 g (1.59 mmol) of $NaNO_2$ in H_2O (20 mL) were added to the residue, 1 N HCl was added dropwise to the mixture cooled to 0 °C until the organic layer turned orange.[18] The CH_2Cl_2 layer was separated, washed with brine, dried ($MgSO_4$), evaporated, and column chromatographed (silica gel, CH_2Cl_2), and recrystallization (EtOH−benzene) gave **2b** in 5.6% yield (60.0 mg, 0.102 mmol) as red prisms: mp >300 °C; IR (KBr) 2980, 2920, 1610, 1440, 1370, 1020, 940, 830, 770, 660, 420 cm^{-1}. Anal. Calcd for $C_{40}H_{40}N_4O_2 \cdot C_6H_6$: C, 80.43; H, 6.75; N, 8.16. Found: C, 80.05; H, 6.72, N; 8.30.

2.4. Analysis of TRESR Spectra of High-Spin Excited States. The spectral simulation was carried out by the eigenfield/exact-diagonalization hybrid method,[19,20] taking electron spin polarization (ESP) into account. The effective exchange interaction between the triplet state of the phenyl- or diphenylanthracene moiety and the dangling radicals is undoubtedly much larger than the Zeeman and fine-structure interactions in the present π-conjugated systems. We can therefore use an ordinary spin Hamiltonian of a pure spin state (negligible quantum mixing of the different spin states) for the analysis, which is given by

$$H'_{spin} = \beta_e \mathbf{B}\cdot\mathbf{g}\cdot\mathbf{S} + \mathbf{S}\cdot\mathbf{D}\cdot\mathbf{S} = \beta_e \mathbf{B}\cdot\mathbf{g}\cdot\mathbf{S} + D[S_Z^2 - S(S+1)/3] + E(S_X^2 - S_Y^2) \quad (1)$$

where **g** and **D** are the electron *g* tensor and fine-structure tensor, respectively. In this effective spin Hamiltonian, the higher order fine-structure terms such as BS^3, S^4, etc. are ignored since these terms, which are allowed group-theoretically, are usually small in magnitude for purely organic molecules consisting of light atoms.

The resonance field $B_{M_S \leftrightarrow M_{S+1}}(\theta,\phi)$ for each transition was directly calculated by solving the following eigenfield equation:[19]

$$A\cdot Z = BC\cdot Z \quad (2)$$

where **A** and **C** are given by the following superoperators:

$$\boldsymbol{A} = \omega E \otimes E - F \otimes E + E \otimes F \quad (3)$$

and

$$\boldsymbol{C} = \boldsymbol{G} \otimes \boldsymbol{E} - \boldsymbol{E} \otimes \boldsymbol{G}^* \quad (4)$$

Here, *E* is a unit matrix and ω is the given microwave frequency. The operators *G* and *F* are the field-dependent and -independent parts of the spin Hamiltonian given in eq 1 ($H'_{spin} = F + BG$), respectively. By solving the above eigenfield equation (eq 2), the resonance field *B* is obtained directly as eigenvalues. The transition probabilities $I(\theta,\phi,\varphi)$ were evaluated by numerically diagonalizing the spin Hamiltonian energy matrix of eq 1, in which the calculated resonance eigenfield was given,[20] where θ, ϕ, and φ are the Euler angles. Since the resonance field is independent of the third Euler angle, φ, the above procedure practically saves the computing time for the simulation. The line-shape function of the TRESR spectrum in the glass matrix is given by

$$g(B) = N\sum\int d\varphi \int d\phi \int d\theta \sin\theta \, P_{M_S \leftrightarrow M_{S+1}}(\theta,\phi)\, I(\theta,\phi,\varphi)\, f[B - B_{M_S \leftrightarrow M_{S+1}}(\theta,\phi)] \quad (5)$$

In this equation, the ESP value between $|S,M_S\rangle$ and $|S,M_{S+1}\rangle$ is expressed by

$$P_{M_S \leftrightarrow M_{S+1}}(\theta,\phi) = P_{M_S} - P_{M_{S+1}} \quad (6)$$

In the simulation, the ESP value on each spin sublevel in zero magnetic field was given as a parameter. A Gaussian function was employed for the line-shape function with a constant line width. The simulation was carried out using a program written by Y.T. on a personal computer.

3. Results and Discussion

3.1. Optical Spectra. UV−vis spectra of **1a**, **1b**, **2a**, and **2b** are shown in Figure 2, along with that of anthracene. The spectral patterns with vibronic splitting in the region of 300−400 nm are very similar to that of anthracene. A slight red shift observed for **1** and **2** was interpreted as the result of π-conjugation between the anthracene moiety and side phenyl rings, and the magnitude of the red shift observed for **1** and **2** was in agreement with that of phenylanthracene or diphenylanthracene. The very broad and weak absorption peaks in the range of 400−500 nm were attributed to a well-known localized nπ*-transition of the dangling iminonitroxide radicals. The nπ* absorption peaks overlap slightly with the absorption due to the anthracene moiety. A strong fluorescence was observed for **1a**, **1b**, **2a**, and **2b** (Figure 3). From the fluorescence spectra, the location of the excited doublet state arising from the $\pi \rightarrow \pi^*$ excitation of the phenyl or diphenylanthracene moiety was determined to be ca. 3.0 eV above the ground state.

3.2. Conventional ESR Spectra. Conventional X-band ESR spectra of **1** and **2** in the ground state are shown in Figure 4. As shown in Figure 4, the ESR spectra of **1a** and **1b** show well-resolved hyperfine splitting arising from the nitrogen atom in the NO group. The temperature dependence of the signal

(19) Belford, G. G.; Belford, R. L.; Burkhalter, J. F. *J. Magn. Reson.* **1973**, *11*, 251.

(20) Teki, Y.; Fujita, I.; Takui, T.; Kinoshita, T.; Itoh, K. *J. Am. Chem. Soc.* **1994**, *116*, 11499. In the spectral simulation of the TRESR spectra, the calculation of ESP has been added as a subroutine to the computer program. More detailed procedures of the spectral simulation for high-spin organic molecules are similar to those described in our previous paper for the perturbation approach: Teki, Y.; Takui, T.; Yagi, H.; Itoh, K.; Iwamura, H. *J. Chem. Phys.* **1985**, *83*, 539.

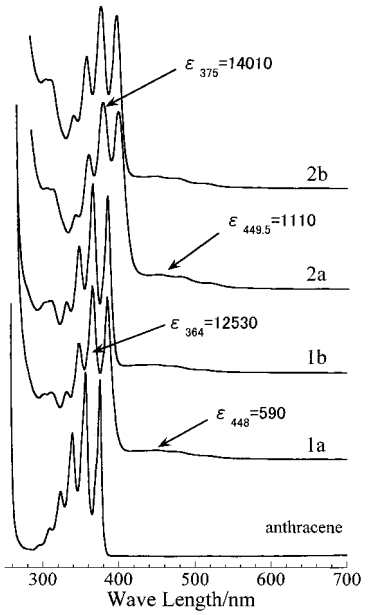

Figure 2. Optical absorption spectra of **1a**, **1b**, **2a**, and **2b** at room temperature. EPA was used for **1a** and **1b,** and 2-MTHF was used for **2a** and **2b** as the solvent. The molar absorption coefficients for **1a** and **2a** are included in the spectra.

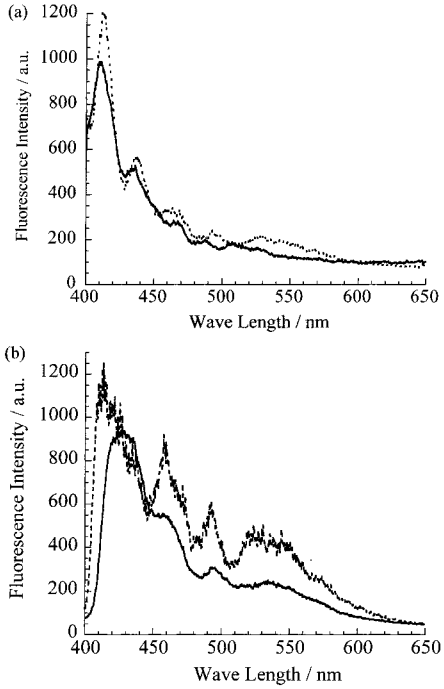

Figure 3. Fluorescence emission spectra of **1a**, **1b**, **2a,** and **2b** observed at 77 K. (a) **1a** (solid line) and **1b** (broken line) in EPA. (b) **2a** (solid line) and **2b** (broken line) in 2-MTHF.

intensity follows simple Curie law. On the other hand in the ESR spectra of **2a** and **2b**, the hyperfine splitting was smeared out and the signal intensities became weak with decreasing temperature. This indicates that a weak intramolecular antiferromagnetic interaction exists between the two dangling iminonitroxide radicals through the ground-state diphenylanthracene moiety as a closed shell spin coupler. To determine the magnitude of the antiferromagnetic intramolecular exchange interaction (J_{intra}), the temperature dependence of the ESR signal intensity (see Figure 4b) was examined in the range of 3−90 K, and the value of J_{intra}/k_B was determined to be -5.8 ± 0.2 K for **2a**. For **2b**, the J_{intra}/k_B value could not be determined accurately, since the magnitude of the exchange interaction was very small.

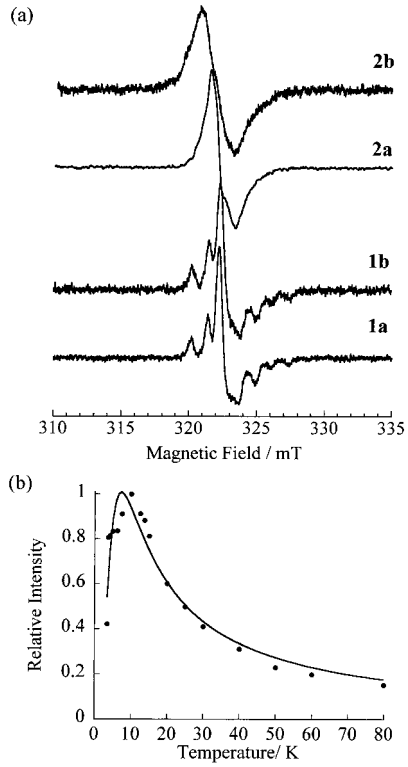

Figure 4. Conventional X-band cw-ESR spectra of **1a**, **1b**, **2a,** and **2b** observed at 30 K in a rigid glass matrix. (a) Observed cw-ESR spectra. The microwave frequencies are 9081.32 MHz for **1a**, 9084.01 MHz for **1b**, 9055.15 MHz for **2a**, 9062.66 MHz for **2b**, respectively. (b) Temperature dependence of the signal intensity of **2a**.

3.3. TRESR Spectra and Excited Spin States of 1a. A typical X-band TRESR spectrum of **1a** observed at 30 K is shown in Figure 5 together with its simulation spectrum. Figure 5a shows the TRESR spectrum of **1a** at 1.0 μs after the laser excitation. The spin Hamiltonian parameters for **1a** determined by the simulation are listed in Table 1, along with those of **2a**. In the present system the triplet state of the phenylanthracene moiety couples with the doublet state of the dangling radical by the spin-exchange interaction. In such an exchange-coupled system the wave function of the whole molecule $|\Psi(S,M)\rangle$ is approximately given by the direct product of the wave functions of the two isolated moieties, $|T(S^A,m_A)\rangle$ and $|R(S^B,m_B)\rangle$, as

$$|\Psi(S,M_S)\rangle = \sum C(S^A S^B S; m_A m_B M)|T(S^A,m_A)\rangle|R(S^B,m_B)\rangle \quad (7)$$

for $S^A = 1$ and $S^B = 1/2$, where $C(S^A S^B S; m_A m_B M)$ is the Clebsch−Gordan coefficient. One quartet (Q) spin state and one doublet (D) spin state were constructed from the radical−triplet pair. The g and D tensors for Q are given by the following:[21]

$$\boldsymbol{g}(Q) = (2/3)\boldsymbol{g}(T) + (1/3)\boldsymbol{g}(R) \quad (8)$$

and

$$\boldsymbol{D}(Q) = (1/3)(\boldsymbol{D}(T) + \boldsymbol{D}(RT)) \quad (9)$$

where $\boldsymbol{D}$(Q), $\boldsymbol{D}$(T), and $\boldsymbol{D}$(RT) are the fine-structure tensors for the excited quartet, the excited triplet, and magnetic dipolar−dipolar interaction between the radical and the excited triplet,

(21) Bencini, A.; Gatteschi, D. *EPR of Exchange Coupled Systems*; Springer-Verlag: Berlin, 1990.

Table 1. *g* Values and Zero-Field Splitting Parameters and ISC Ratio of the Quartet (Q) and the Quintet (Qu) Excited States

	g	D/cm^{-1}	E/cm^{-1}	ISC ratio
Q of **1a**	2.0043	0.0235	0.0	$P_{+3/2'}:P_{+1/2'}:P_{-1/2'}:P_{-3/2'} = 0.0:0.5:0.5:0.0$
Qu of **2a**	2.0043	0.0130	0.0	$P_{+2'}:P_{+1'}:P_{0'}:P_{-1'}:P_{-2'} = 0.0:0.35:0.30:0.\ 35:0.0$

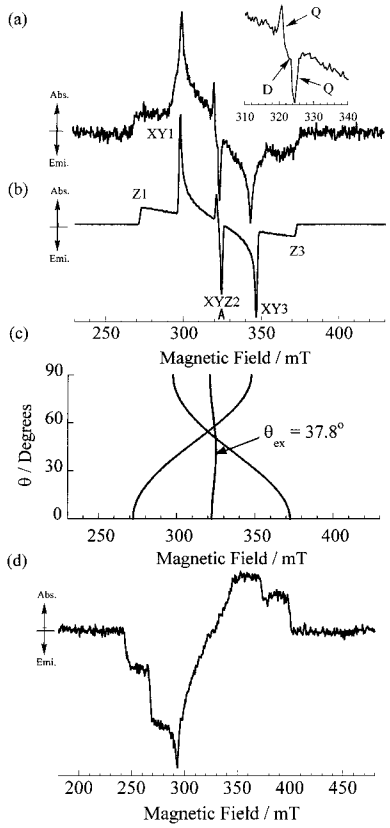

Figure 5. Typical TRESR spectra of **1a** and anthracene at 30 K in an EPA rigid glass matrix. The microwave frequencies are 9040.6 MHz for **1a** and 9030.6 MHz for anthracene. (a) Observed spectrum of **1a** at 1.0 μs after laser excitation. The inset shows an expanded spectrum in the $g \approx 2$ region. In the inset Q and D denote the signals due to the excited quartet and doublet states, respectively. (b) Simulated spectrum of the excited quartet state using the spin Hamiltonian parameters described in text. The line width ΔB_{msl} was determined to be 0.7 mT by the simulation. Here, X, Y, and Z are the signals corresponding to the canonical orientation of the fine-structure tensor. "A" denotes the off-axis extra line, and θ_{ex} indicates the angle corresponding to the extra line.[38] (c) Calculated angular dependence of the resonance field. (d) Observed spectrum of anthracene at 1.0 μs after laser excitation.

respectively. For D arising from the radical−excited triplet pair, the *g* tensor is given by[21]

$$\boldsymbol{g}(\mathrm{D}) = (4/3)\boldsymbol{g}(\mathrm{T}) - (1/3)\boldsymbol{g}(\mathrm{R}) \qquad (10)$$

From eq 8, the averaged *g* value for the excited quartet state of **1a** was estimated to be $g(\mathrm{Q}) = 2.004_0$ using the *g* values of the iminonitroxide radical ($g(\mathrm{R}) = 2.006$)[22] and the excited $\pi\pi^*$ triplet state of free anthracene ($g(\mathrm{T}) = 2.003$). The fine-structure parameter *D* of the excited quartet state was also estimated to be $D(\mathrm{Q}) = 0.0256$ cm^{-1} from eq 9 using $D(\mathrm{T}) = 0.0710$ cm^{-1} of the excited triplet state of free anthracene[23] and $D(\mathrm{RT}) = (3/2)D_{ZZ}(\mathrm{RT}) = 0.0057$ cm^{-1} calculated by the point dipole approximation. Here D_{ZZ}(RT) is the matrix element of $\boldsymbol{D}$(RT) in the direction along the *Z* principal axis of $\boldsymbol{D}$(Q), which is approximated to be parallel to the direction for $\boldsymbol{D}$(T) to give the largest fine-structure splitting because $|\boldsymbol{D}(\mathrm{T})| \gg |\boldsymbol{D}(\mathrm{RT})|$. In this estimation, we used the *D* value of anthracene instead of the value for phenylanthracene, since the *D* value of the T_1 state of phenylanthracene was unknown. It was impossible to detect the T_1 state of phenylanthracene due to the low efficiency of intersystem crossing from S_0 to the T_1 state. The experimentally determined *g* and *D* values for the excited quartet states of **1a** ($g(\mathrm{Q}) = 2.0043$ and $D(\mathrm{Q}) = 0.0235$ cm^{-1}) shown in Table 1 are in excellent agreement with the calculations.[24] This means that the excited quartet state was generated by the spin-exchange coupling between the $\pi\pi^*$ excited triplet state of the diphenylanthracene moiety and the doublet ground state of the dangling stable radical. The observed TRESR shows an A/E pattern as shown in Figure 5a. The relative populations (polarization) of each M_S sublevel in Q have been determined to be $P_{+1/2'} = P_{-1/2'} = 0.5$ and $P_{+3/2'} = P_{-3/2'} = 0.0$ with an increasing order of energy in zero magnetic field from the spectral simulation shown in Figure 5b. Here, we assumed that $D > 0$, because Q is expected to have the same sign of *D* as that of the triplet state of anthracene according to eq 9. The relative populations show that a selective intersystem crossing (ISC) to the $M_S = \pm 1/2$ sublevels occurs from the $\pi\pi^*$ excited doublet state (D_n). Hereafter, D_n stands for the photoexcited doublet state arising from the radical−excited singlet pair in which the dangling iminonitroxide radical couples with the photoexcited $\pi\pi^*$ singlet state of the phenylmethylene moiety generated by a vertical $\pi \rightarrow \pi^*$ photoexcitation. The observed ESP is discussed in section 3.7.

The signal with emissive polarization (E), which can be attributable to the excited doublet state, D, arising from the radical−excited triplet pair, was very weak (see the inset in Figure 5a). The *g* value for D was determined to be $g(\mathrm{D}) = 2.002 \pm 0.001$, which is in agreement with the value of 2.002_0 estimated using eq 10. As pointed out in the case of the excited doublet and quartet states of ZnTPP−nitpy,[8b] the emissive polarization indicates that the energy level of the excited quartet state is lower than that of the excited doublet spin state. Therefore, the sign of the exchange interaction between the excited triplet state ($S = 1$) of the anthracene moiety and the doublet spin state ($S = 1/2$) of the dangling iminonitroxide radical would be positive (ferromagnetic). The positive sign also supported by the theoretical calculations will be discussed in section 3.9. The weak signal due to the excited doublet state can be explained in terms of a large energy separation between Q and D due to a larger spin-exchange interaction because the ESP of the excited doublet state is generated from the perturbed mixing of the quartet wave functions ($|\mathrm{Q},\pm 1/2'\rangle$) with the doublet wave functions ($|\mathrm{D},\pm 1/2'\rangle$). The larger spin-exchange interaction arises from the π-conjugation. Thus, in the excited quartet state, an intramolecular ferromagnetic spin alignment between the excited triplet chromophore and the dangling radical spin occurs through spin polarization in the dangling phenyl

(22) The *g* value and isotropic hyperfine coupling constants of the two nitrogen atoms were determined to be $g = 2.0060$, $a_N(1) = 0.92$ mT, and $a_N(2) = 0.42$ mT from simulation of the room-temperature ESR spectrum of 1a in toluene solution, although in our previous paper[2] $g = 2.007$, which was an averaged value for the various nitroxide radicals, was used.

(23) The *g*, *D*, and *E* values for the T_1 state of anthracene in an EPA rigid glass matrix were determined to be $g = 2.003$, $D = 0.0710$ cm^{-1}, and $E = 0.0070$ cm^{-1}. Also the relative populations of the sublevels were $P_X = 0.45$, $P_Y = 0.55$, and $P_Z = 0.0$.

(24) Since the π spin density on phenyl or diphenylanthracene is slightly delocalized to the phenyl ring, an estimated value of *D* is slightly smaller.

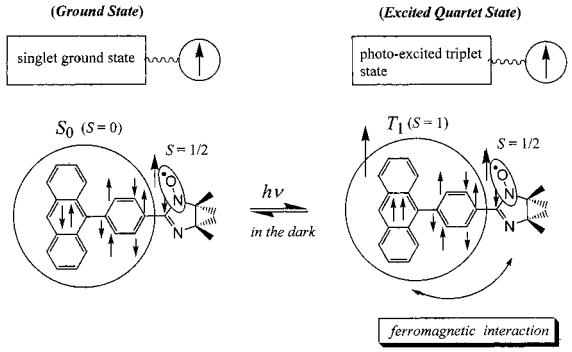

Figure 6. Schematic diagram of the spin alignment in the doublet ground state and the excited quartet state of **1a**. In the ground state, the radical spin couples with the closed-shell singlet state of the phenylanthracene moiety. On the other hand, in the photoexcited states, the radical spin couples ferromagnetically with the triplet excited state of the phenylanthracene moiety by the spin polarization through π-conjugation.

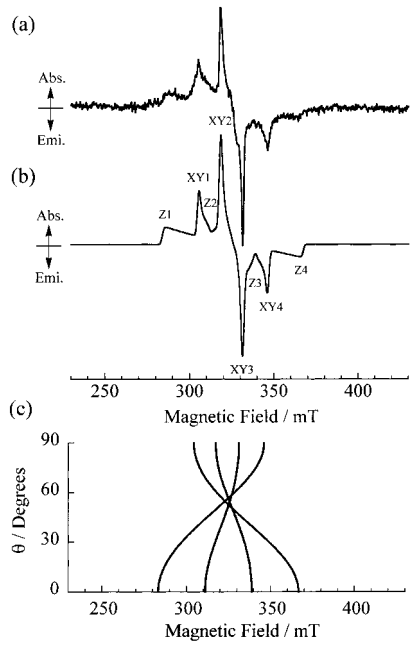

Figure 7. Typical TRESR spectra of 2a at 30 K in a 2-MTHF rigid glass matrix. The microwave frequency is 9135.7 MHz. (a) Observed spectrum at 30 K and 1.0 μs after laser excitation. (b) Simulation of the excited quintet spectrum using the spin Hamiltonian parameters described in text. The line width ΔB_{msl} was also determined to be 0.7 mT by the spectral simulation. (c) Calculated angular dependence of the resonance field.

group shown in Figure 6. The details of the spin alignment are discussed in section 3.8.

3.4 TRESR Spectra and Excited Spin States of 2a. A typical TRESR spectrum of **2a** observed at 30 K is shown in Figure 7 together with its simulation spectrum. Figure 7a shows the TRESR spectrum observed at 1.0 μs after the laser excitation. The spin Hamiltonian parameters determined by the spectral simulation are listed in Table 1. The observed TRESR shows an A/E pattern (Figure 7a), and the determined relative populations (polarization) of each M_S sublevel in the quintet state (Qu) are also shown in Table 1. The relative population shows that the selective ISC to the $M_S = 0, \pm 1$ sublevels occurs from the $\pi\pi^*$ excited singlet state (S_n) which is generated by the $\pi \rightarrow \pi^*$ photoexcitation of the diphenylanthracene moiety.

The triplet state of the diphenylanthracene moiety couples with the doublet state of the two dangling stable radicals. In

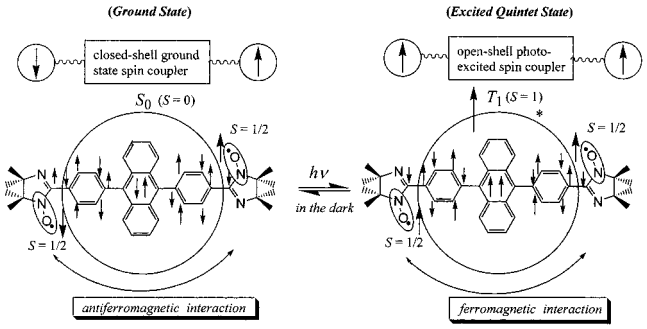

Figure 8. Schematic diagram of the spin alignment utilizing the excited triplet molecular field in **2a**. In the ground state, the spin polarization mechanism is dominant, leading to the antiferromagnetic coupling between the two dangling radical spins, because the diphenylanthracene spin coupler is a closed shell. On the other hand, in the photoexcited states, the spin delocalization mechanism overcomes the spin polarization effect in the anthracene moiety, because the spin coupler becomes an open-shell triplet excited state. This leads to the ferromagnetic coupling between the two dangling radical spins in the photoexcited state.

this exchange-coupled system, the wave function for the whole molecule $|\Psi(S,M)\rangle$ is given approximately as a direct product of the wave functions for the three isolated moieties, $|T(S^A,m_A)\rangle$, $|R_1(S^B,m_B)\rangle$, and $|R_2(S^B,m_B)\rangle$ using Racah coefficients. According to the projection theorem of the angular momentum,[25] the D tensor for Qu is obtained using the D tensor for the excited triplet state of the isolated anthracene moiety and the dipolar interaction between the radical and the excited triplet by

$$\boldsymbol{D}(\mathrm{Qu}) = (1/6)(\boldsymbol{D}(\mathrm{T}) + \boldsymbol{D}(\mathrm{R_1T}) + \boldsymbol{D}(\mathrm{R_2T})) \qquad (11)$$

Here, the contribution arising from the direct dipolar interaction between the dangling radical spins is ignored because the values are 2 orders of magnitude smaller than the intrinsic fine-structure interaction of the excited triplet anthracene moiety. Under the similar approximation used in the case of the quartet state, the fine-structure parameter D of the quintet state was estimated to be $D(\mathrm{Qu}) = 0.0137$ cm^{-1} from eq 11, using $D(\mathrm{T}) = 0.0710$ cm^{-1} for the excited triplet state of free anthracene and $D(\mathrm{R_1T}) = D(\mathrm{R_2T}) = 0.0057$ cm^{-1} calculated in the direction of the Z principal axis of $\boldsymbol{D}$(Qu) by the point dipole approximation. The experimentally determined D value (0.0130 cm^{-1}) for the quintet state of **2a** is in excellent agreement with the calculation, indicating that the observed excited quintet state ($S = 2$) arises from a $\pi\pi^*$ excited triplet state of the diphenylanthracene moiety and two dangling radical spins.

The clear detection of the excited quintet ($S = 2$) state indicates that the intramolecular ferromagnetic (parallel) spin alignment between the two doublet spins ($S = 1/2$) in the dangling phenyl iminonitroxide radicals is realized by the photoexcited triplet ($S = 1$) molecular field of the diphenylanthracene moiety. Since there is no reason for the different sign of the exchange coupling for **2a**, it was concluded that the sign of the exchange interaction is also ferromagnetic in **2a**. Thus, the intramolecular ferromagnetic exchange interaction among the excited triplet chromopore and two dangling radicals arises in **2a**.

Figure 8 shows the schematic diagram of the spin alignment utilizing the excited molecular field in **2a**. There are two dominant mechanisms for the intramolecular spin alignment. One is a spin polarization mechanism, and the other is a spin

(25) (a) Rose, M. E. *Elementary Theory of Angular Momentum*; John Wiley & Sons: New York, 1957. (b) Judd, B. R. *Operator Techniques in Atomic Spectroscopy*; McGraw-Hill: New York−San Francisco−Toronto−London, 1963.

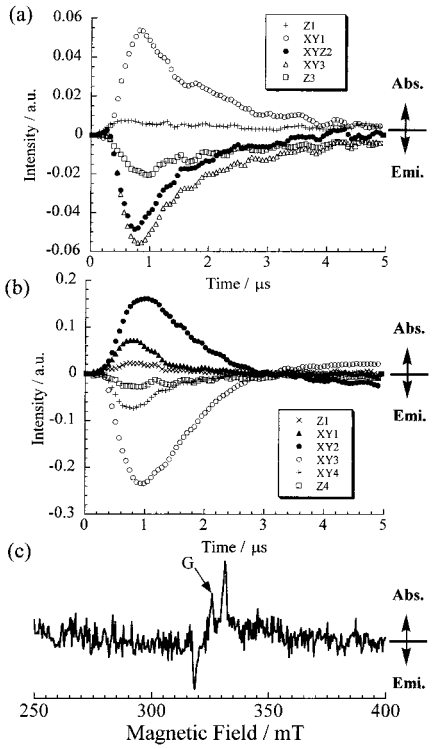

Figure 9. Time profiles observed at each canonical resonance field of the fine-structure transitions of (a) the excited quartet state of **1a** and (b) the excited quintet state of **2a**. Assignment of each transition is shown in Figures 5 and 7. The time profiles were observed at 30 K. (c) TRESR spectrum of **2a** observed at 4 μs after the laser excitation. The signal indicated by "G" may come from the ground state.

delocalization mechanism.[26] The ferromagnetic spin alignment in **2a** in the excited state shows that the spin delocalization mechanism is much more dominant than in the ground state. Since **2a** is a symmetrical diradical, the spin polarization mechanism leads to an antiferromagnetic spin configuration between the dangling radicals, according to the topological rule for the π-electron network.[11−15] Actually, a weak antiferromagnetic exchange interaction was observed for this system in the ground state as described in section 3.2 because the diphenylanthracene moiety has a closed-shell spin configuration in the ground state as shown in Figure 8. However, in the open-shell T_1 state of the anthracene moiety, the spin delocalization mechanism would overcome the spin polarization effect as shown in section 3.9. This leads to a large positive spin density at the symmetrical carbon positions, 9 and 10, of the anthracene moiety. As a result, all unpaired spins in the photoexcited state of **2a** are parallel to each other, giving an excited quintet high-spin state ($S = 2$) as shown in Figure 8. As already pointed out in our previous paper,[2] these results show that the sign of the effective exchange coupling between two dangling stable radicals through the spin coupler becomes ferromagnetic through the photoexcitation. The spin distribution, which is shown in section 3.9, confirms this finding. Thus, the photoinduced spin alignment utilizing the excited triplet molecular field of the purely organic π-conjugated system has been achieved for the first time in this spin system (Figure 8). A similar phenomenon has been very recently reported in a covalently linked (σ-conjugated) binitroxide−fullerene derivative system.[10b]

3.5. Time Profiles of the Observed High-Spin Excited States. The time profiles for the TRESR signals of **1a** and **2a** at each canonical resonance position of the fine-structure tensor are shown in parts a and b, respectively, of Figure 9. All canonical transitions in the observed TRESR spectrum of **1a** in Figure 5a show a similar time−decay behavior, indicating that all signals come from a unique quartet spin state. The dynamic electron spin polarization decayed within 10 μs, and no further signals could be detected after 10 μs. Although the time profile of a very weak doublet, shown by arrow D in the inset of Figure 5a, could not be clearly detected, it seemed to decay more rapidly than the quartet signals. The ESP of Qu also decayed within 10 μs, and all canonical transitions in the observed TRESR spectrum of **2a** (Figure 7a) showed a similar time−decay behavior (Figure 9b). No other signals arising from different excited spin states were detected during the decay time of ESP, suggesting that the excited triplet species arising from the radical−triplet−radical system of **2a** decayed rapidly within 0.2 μs or the population was less than the sensitivity of our TRESR spectrometer. Furthermore, an inversion of the ESP signal was observed for **2a** in the long time region ($t > 3.5$ μs). This finding shows that selective ISC toward the ground state occurs from the $M_S = \pm 1$ and 0 sublevels of the quintet state, in a similar manner to the selective ISC from the S_n state mentioned above. In addition, the absorptive (A) doublet-like signal of the ground state (G) (Figure 9c) appears with weak signal intensity in the longer time region. This signal may be assigned to the lowest triplet state (T_0) polarized by an ISC from Qu to T_0, which is closely located above the singlet ground state (S_0) (section 3.2).

3.6. Spin−Orbit Wave Functions of the Ground and Excited Spin States. To discuss the mechanism of the dynamic ESP, the spin−orbit wave functions were investigated. For the convenience of this discussion, the direct products of the wave functions for the isolated phenylanthracene/diphenylanthracene moiety and the iminonitroxide radicals were approximately used for the wave function for the whole molecule. The wave functions are assumed to be orthogonal to each other although they are actually slightly mixed through π-conjugation. The mixing is considered in the later discussion. Only the highest occupied MO (π-HOMO) and the lowest unoccupied MO (π^*-LUMO) of phenyl- and diphenylanthracene moieties, the singly occupied MOs (SOMOs) of the radicals, and the lone-pair nonbonding orbital at the oxygen sites were treated. R and n denote the SOMO of the radical and the nonbonding lone-pair orbital of the oxygen site, respectively. Hereafter, we give only the explicit expressions for the spin−orbit wave functions of the ground and excited states that play important roles in the generation of ESP in our systems, even though there are various excited states constructed from π, π^*, R, and n.

Spin−Orbit Wave Functions of 1a. According to the antisymmetrical requirement for the total wave function with respect to permutation of any pair of electrons and the requirement of the good quantum numbers of S and S_Z (eq 7), the wave functions are written using Slater determinants. The spin−orbit wave functions for the electronic ground state are

$$|D_0,+1/2\rangle = |\pi\bar{\pi}R\bar{n}n| \quad (12a)$$

$$|D_0,-1/2\rangle = |\bar{\pi}\pi R\bar{n}n| \quad (12b)$$

The wave functions of the excited doublet states constructed from the first $\pi\pi^*$ excited singlet state of the phenylanthracene moiety and the ground-state doublet of the dangling radical are

$$|D_n,+1/2\rangle = (1/\sqrt{2})(|\pi\bar{\pi}^*R\bar{n}n| - |\bar{\pi}\pi^*R\bar{n}n|) \quad (13a)$$

$$|D_n,-1/2\rangle = (1/\sqrt{2})(|\bar{\pi}\pi^*R\bar{n}n| - |\bar{\pi}\pi^*R\bar{n}n|) \quad (13a)$$

The $\pi\pi^*$ excited doublet state is 3.02 eV above the ground state. This was determined by the fluorescence spectrum. The Q state constructed from the $\pi\pi^*$ excited triplet state and the dangling radical was detected by TRESR. The spin−orbit wave functions

(26) Yamashita, S.; Okamura, M.; Nagao, H.; Yamauchi, K. *Chem. Phys. Lett.* **1995**, *233*, 88.

are

$$|Q_{\pi\pi^*},+3/2\rangle = |\pi\pi^*Rn\bar{n}| \quad (14a)$$

$$|Q_{\pi\pi^*},+1/2\rangle = (1/\sqrt{3})(|\pi\pi^*\bar{R}n\bar{n}| + |\pi\overline{\pi^*}Rn\bar{n}| + |\bar{\pi}\pi^*Rn\bar{n}|) \quad (14a)$$

$$|Q_{\pi\pi^*},-1/2\rangle = (1/\sqrt{3})(|\overline{\pi\pi^*}Rn\bar{n}| + |\pi\overline{\pi^*R}n\bar{n}| + |\bar{\pi}\pi^*\bar{R}n\bar{n}|) \quad (14c)$$

$$|Q_{\pi\pi^*},-3/2\rangle = |\overline{\pi\pi^*Rn}\bar{n}| \quad (14d)$$

UHF ab initio calculation of **1a** (not shown) using the Becke3LYP density functional theory (DFT) indicated that the $\pi\pi^*$ excited quartet state is the lowest quartet state. A charge-transfer (CT)-type nπ^* excited quartet state constructed from the dangling radical SOMO and a CT-type nπ^* excited triplet state arises from the one-electron transfer from the lone pair of the oxygen atom to the π^*-orbital of the phenylanthracene. The CT-type nπ^*-state is different from the nπ^*-state localized on the radical site.[27] The spin−orbit wave functions are

$$|Q_{n\pi^*},+3/2\rangle = |\bar{\pi}\pi\pi^*Rn| \quad (15a)$$

$$|Q_{n\pi^*},+1/2\rangle = (1/\sqrt{3})(|\pi\bar{\pi}\pi^*\bar{R}n| + |\pi\overline{\pi\pi^*}Rn| + |\bar{\pi}\pi\pi^*\bar{R}n|) \quad (15b)$$

$$|Q_{n\pi^*},-1/2\rangle = (1/\sqrt{3})(|\overline{\pi\pi\pi^*}\bar{R}n| + |\pi\,\overline{\pi\pi^*R}n| + |\pi\bar{\pi}\pi^*\overline{R}n|) \quad (15c)$$

$$|Q_{n\pi^*},-3/2\rangle = |\overline{\pi\pi\pi^*Rn}| \quad (15d)$$

The $Q_{n\pi^*}$ state can mix with the $Q_{\pi\pi^*}$ state through π-conjugation, causing the ESP in the observed Q state. In addition to these states, it is necessary to consider the following photoinduced CT excited doublet state:

$$|D_{CT}^*,+1/2\rangle = |\pi\bar{\pi}\pi^*\bar{n}n| \quad (16a)$$

$$|D_{CT}^*,-1/2\rangle = |\pi\overline{\pi\pi^*}\bar{n}n| \quad (16b)$$

In this CT state, one electron is transferred from the SOMO of the radical to the phenylanthracene moiety. Unfortunately, the CT state could not be clearly observed in the optical spectra. However, this is not in conflict with our consideration described later because the CT absorption will overlap with the observed transitions and has much smaller intensity.

Spin−Orbit Wave Functions of 2a. The spin−orbit wave functions of the ground state and various excited states were constructed using the π- and π^*-orbitals of the diphenylanthracene moiety and the SOMOs of the two dangling radicals (R_1 and R_2). The spin−orbit wave functions of the $\pi\pi^*$ excited quintet state ($S = 2$), which was detected by TRESR experiments, are

$$|Qu_{\pi\pi^*},+2\rangle = |\pi\pi^*R_1R_2\bar{n}\bar{n}| \quad (17a)$$

$$|Qu_{\pi\pi^*},+1\rangle = (1/2)(|\pi\pi^*R_1\bar{R}_2\bar{n}\bar{n}| + |\pi\overline{\pi^*}R_1R_2\bar{n}\bar{n}| + |\bar{\pi}\pi^*R_1R_2\bar{n}\bar{n}| + |\bar{\pi}\pi^*R_1R_2\bar{n}\bar{n}|) \quad (17b)$$

$$|Qu_{\pi\pi^*},0\rangle = (1/\sqrt{6})(|\pi\pi^*\overline{R_1R_2}\bar{n}\bar{n}| + |\pi\,\overline{\pi^*R_1R_2}\bar{n}\bar{n}| + |\overline{\pi\pi^*R_1}R_2\bar{n}\bar{n}| + |\bar{\pi}\pi^*R_1\bar{R}_2\bar{n}\bar{n}| + |\bar{\pi}\pi^*\bar{R}_1R_2\bar{n}\bar{n}| + |\overline{\pi\pi^*}R_1R_2\bar{n}\bar{n}|) \quad (17c)$$

$$|Qu_{\pi\pi^*},-1\rangle = (1/2)(|\overline{\pi\pi^*R_1R_2}\bar{n}\bar{n}| + |\bar{\pi}\pi^*\overline{R_1R_2}\bar{n}\bar{n}| + |\overline{\pi\pi^*}R_1\bar{R}_2\bar{n}\bar{n}| + |\overline{\pi\pi^*R_1}R_2\bar{n}\bar{n}|) \quad (17d)$$

$$|Qu_{\pi\pi^*},-2\rangle = |\overline{\pi\pi^*R_1R_2}\bar{n}\bar{n}| \quad (17e)$$

The explicit expressions of the spin−orbit wave functions of other spin states were obtained in a manner similar to that of **1a** (not included).

3.7. Selective Enhanced Intersystem Crossing and Electron Spin Polarization for High-Spin Excited States. ESP Generation Mechanism of 1a. The relative populations (polarizations) of each M_S sublevel in Q have been determined to be $P_{+1/2'} = P_{-1/2'} = 0.5$ and $P_{+3/2'} = P_{-3/2'} = 0.0$ with an increasing order of energy in zero magnetic field from the spectral simulation shown in Figure 5b.[28] As shown in Figure 10, this ESP pattern can be interpreted by assuming an M_S conserved selective ISC ($D_n \rightarrow Q_{\pi\pi^*}$) between the $M_S = \pm 1/2$ sublevels of D_n and $Q_{\pi\pi^*}$ in zero magnetic field. The origin of the ISC should be attributed to the spin−orbit coupling (SOC) of the dangling N−O group for the following reasons: (i) The possibility of a dominant ISC process by a dipolar mixing between $D_{\pi\pi^*}$ and $Q_{\pi\pi^*}$ was easily ruled out because the magnitude of the intramolecular exchange interaction (J) is much larger than that of the dipolar interaction (D) in the π-conjugated spin systems.[29] (ii) It is known that diphenylanthracene has a very low efficiency for ISC from S_1 to T_1.[30] (iii) There are no atoms, other than the oxygen in the radical, with localized unpaired electrons that have large SOC. Thus, for understanding of the selective ISC in our systems, it is necessary to consider an enhanced ISC mechanism, which is caused by the presence of a dangling radical with a 1/2 spin.

The most plausible mechanism for the dynamic ESP is an intramolecular electron transfer (ET) through π-conjugation and SOC on the local N−O group (Figure 11).[31] Direct SOC between the D_n and $Q_{\pi\pi^*}$ states vanishes because the SOC Hamiltonian, H_{SO}, is a one-electron operator, and SOC between the D_n and $Q_{\pi\pi^*}$ states is also negligible as a result of the symmetry between $|D_n,\pm 1/2\rangle$ and $|Q_{\pi\pi^*},\pm 3/2\rangle$.[32] On the other hand, the SOC interaction between the $M_S = \pm 1/2$ sublevels of $Q_{n\pi^*}$ ($|Q_{n\pi^*},\pm 1/2\rangle$) and the charge-transfer state ($|D_{CT}^*,\pm 1/2\rangle$) in eqs 16a and 16b has a large matrix element which is given as follows:

$$\langle D_{CT}^*,\pm 1/2|H_{SO}|Q_{n\pi^*},\pm 1/2\rangle = (1/\sqrt{3})\xi\langle n|l_Z|R\rangle \approx (1/\sqrt{3})\xi\gamma\langle n|l_Z|p\pi(O)\rangle \quad (18)$$

All other matrix elements are insignificant. Here, the Z axis was chosen to be along the N−O bond axis, and γ is a coefficient of the pπ orbital for the oxygen atom in the SOMO.[33] The magnitude of γ is roughly estimated to be ca. 0.57 from the ab initio MO calculation (STO-3G basis set).[34] Equation 18 shows that the SOC leads to a selective ISC from D_{CT}^* to $|Q_{n\pi^*},\pm 1/2\rangle$. ESP transfer from $Q_{n\pi^*}$ to $Q_{\pi\pi^*}$ occurs easily since

(27) The quartet TRESR spectrum was also observed by the photoexcitation to the localized nπ^*-state using 445 nm light from OPO (Continuum Surelite OPO) pumped by a YAG laser. This finding indicates that the localized nπ^*-state is higher in energy than the nπ^* (CT-type) and $\pi\pi^*$ quartet states because the energy transfer occurs from higher energy states toward lower energy states. Since the $\pi\pi^*$ doublet excited state exists higher in energy than the localized nπ^*-state, as shown in the optical spectra of **1** and **2** in Figure 2, the nπ^* (CT-type) and $\pi\pi^*$ quartet states are lower in energy than the $\pi\pi^*$ doublet excited state.

(28) For $P_{+1/2'}$, $P_{-1/2'}$, $P_{+3/2'}$, and $P_{-3/2'}$, we employed the same notation used in the work of Ishii et al.[8b]

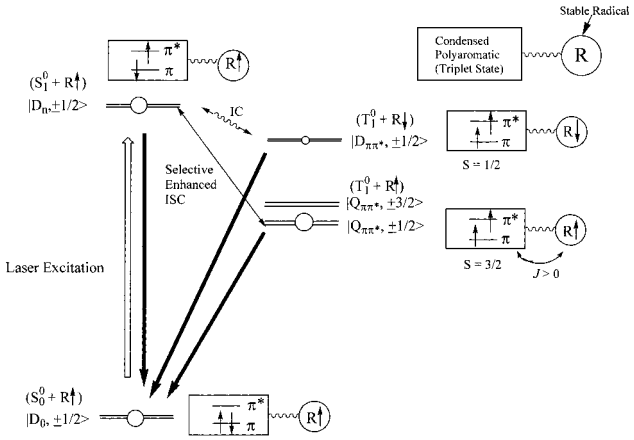

Figure 10. Schematic illustration of the energy diagram, selective intersystem crossing, and energy relaxation process. The $M_S = \pm 1/2$ sublevels of the quartet state are selectively populated by ISC. In this diagram, R is the doublet ground state of the isolated dangling radical. S_0^0, S_1^0, and T_1^0 are the ground and the excited singlet and triplet states of the phenylanthracene moiety, respectively.

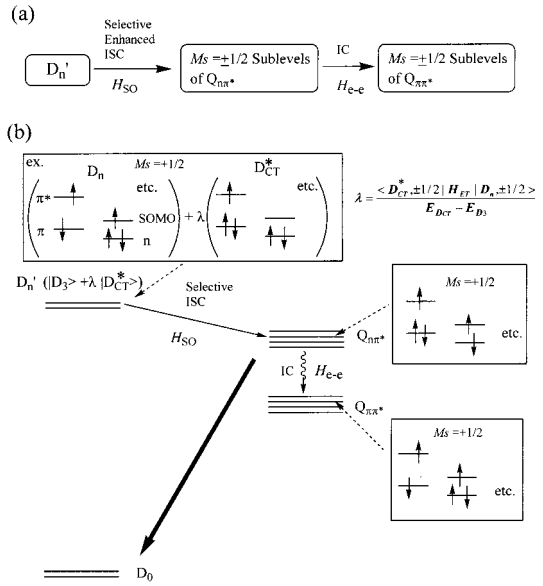

Figure 11. Most plausible mechanism for the dynamic electron spin polarization of the quartet excited state (Q). (a) Selective intersystem crossing from the perturbed excited doublet state (D_n') to the $M_S = \pm 1/2$ sublevels of the $n\pi^*$ quartet state ($Q_{n\pi^*}$) followed by the internal conversion to the observed $\pi\pi^*$ quartet excited state ($Q_{\pi\pi^*}$). (b) Schematic illustration of the energy diagram and the ESP transfer process. Only the $M_S = \pm 1/2$ sublevels of $Q_{n\pi^*}$ have a nonzero SOC matrix element (H_{SO}) with the component of the CT state in the perturbed doublet state (D_n') (see the text). The ESP generated in $Q_{n\pi^*}$ is transferred to $Q_{\pi\pi^*}$ through the IC process induced by the electronic coupling (H_{e-e} = electron transfer or exchange interaction). A typical spin configuration of $M_S = +1/2$ sublevel is also shown as an example.

this process is an internal conversion between states with the same spin multiplicity. In this process, the ESP of $Q_{n\pi^*}$ is conserved in $Q_{\pi\pi^*}$, since $|\langle Q_{n\pi^*},M_S|H|Q_{\pi\pi^*},M_S\rangle| \neq 0$ only between the spin sublevels with the same M_S values. In addition, the $n\pi^*$ excited state is expected to be located slightly above the $\pi\pi^*$ excited quartet state. The small nonvanishing matrix element between $Q_{n\pi^*}$ and $Q_{\pi\pi^*}$ causes mixing of both states. Therefore, if there is any nonzero matrix element between the D_n and D_{CT}^* states, selective ISC occurs from D_n to the $M_S = \pm 1/2$ sublevels of Q ($|Q_{\pi\pi^*},\pm 1/2\rangle$), according to the pathway in Figure 11a. The most reasonable candidate is an ET interaction (H_{ET}) from the SOMO of the radical to the π-HOMO of the phenylanthracene moiety. The matrix element is roughly estimated by

$$\langle H_{ET}\rangle_{D_n \to CT} = |\langle D_{CT}^*,\pm 1/2|H|D_n,\pm 1/2\rangle| \approx (1/\sqrt{2})|\langle \pi|H|R\rangle| \quad (19)$$

Since the π-HOMO interacts with the radical site through π-conjugation, this matrix element has a large value, leading to the mixing between the D_n and D_{CT}^* states. According to first-order perturbation theory, the perturbed doublet state (D_n') is described by[35]

$$|D_n'\pm 1/2\rangle = |D_n^0,\pm 1/2\rangle + \frac{\langle D_{CT}^*,\pm 1/2|H|D_n,\pm 1/2\rangle}{E_{CT} - E_{D_n}}|CT,\pm 1/2\rangle \quad (20)$$

This state has a nonzero matrix of the SOC for $|Q_{n\pi^*},\pm 1/2\rangle$, which leads to selective ISC from D_n to $Q_{n\pi^*}$ (Figure 11b). According to the M_S conservation rule, the ESP of $Q_{n\pi^*}$ is transferred to the $M_S = \pm 1/2$ sublevels of $Q_{\pi\pi^*}$ ($|Q_{\pi\pi^*},\pm 1/2\rangle$) through an energy-transfer process. This process may be the most plausible mechanism for the enhanced selective ISC between D_n and the observed $\pi\pi^*$ quartet states ($Q_{\pi\pi^*}$). However, we cannot completely rule out the possibility of another ESP mechanism because no direct evidence for the D_{CT}^* state was obtained from optical spectra.

ESP Generation Mechanism of 2a. In a manner similar to that of **1a**, the ESP for Qu in **2a** can be interpreted as a selective enhanced ISC ($S_n \rightarrow Qu$) (Figure 12) generated through SOC on the N−O groups. However, the quantitative calculation for the ESP for Qu is much more difficult than for $Q_{\pi\pi^*}$. In an alternative way, the dominant ESP of Qu was estimated by assuming the quintet state as an exchange-coupled spin system

(29) The value of J_{intra}/k_B was determined to be -5.8 ± 0.2 K for the ground state of **2a** as described in section 3.2. The magnetic interaction arises from the indirect interaction through the closed-shell anthracene moiety. The magnitude of the direct exchange interaction through π-conjugation between the radical and the open-shell triplet state of the anthracene moiety is expected to be much larger, though the magnitude of the intramolecular exchange interaction on the photoexcited states of **1a** was not determined.

(30) Actually, the direct detection via TRESR of the T_1 state of phenylanthracene was not successful under the same conditions used to detect the quartet state.

(31) A novel spin polarization mechanism by an intramolecular photo-induced energy transfer and the selective enhanced intersystem crossing were recently reported in a covalently linked copper(II) porphyrin−free-base porphyrin dimer: (a) Asano-Someda, M.; van der Est, A.; Krüger, U.; Stehlik, D.; Kaizu, Y.; Levanon, H. *J. Phys. Chem. A* **1999**, *103*, 6704. (b) Toyama, N.; Asano-Someda, M.; Ichino, T.; Krüger, Kaizu, Y. *J. Phys. Chem. A* **2000**, *104*, 4857. However, the mechanism works in the case of quantum mixing in the triplet−doublet pair and cannot be straightforwardly applicable to our system since the spin states in our systems are pure spin states, indicating negligible quantum mixing.

(32) The negative sign between two Slater determinants in eq 13 and positive sign for the same Slater determinants in eq 14.

(33) It is well-known that N−O radicals have the largest g value for this direction along the N−O bond axis and the magnitude is typically $g_{ZZ} = 2.010$. (Capiomont, A.; Chion, B.; Lajzerowicz-Bonneteau, J.; Lemaire, H. *J. Chem. Phys.* **1974**, *60*, 2350. In this paper, the X direction has been chosen along the N−O bond axis.) For the other two directions, g_{YY} is 2.007 and g_{XX} is 2.003 (pπ-direction) typically. The large deviation of g_{ZZ} from the free spin g value means that the SOC matrix element ($\xi\langle n|l_Z|p\pi(O)\rangle$) between the lone pair orbital (n) and the pπ-orbital on the oxygen site does not vanish and the other SOC elements are negligible.

(34) The STO-3G minimum basis set was used since the use of the larger basis sets gave more than one set of artificial p-orbitals, complicating the estimation.

(35) Since the quantitative estimation of the matrix element in eq 20 is actually very difficult, it is not presented in this paper, even though it can help to validate the proposed mechanism.

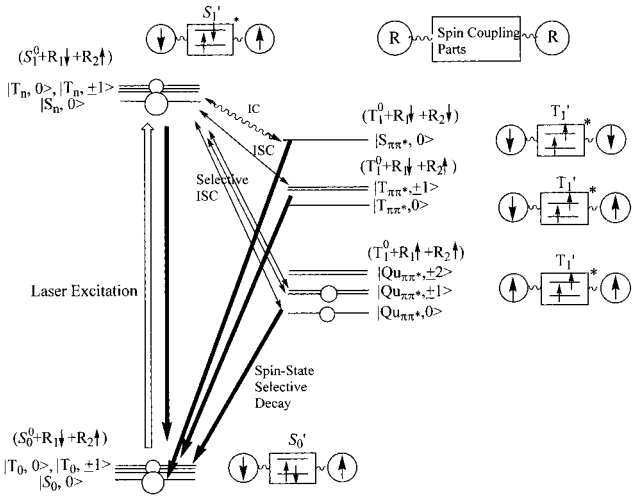

Figure 12. Schematic illustration of the energy diagram, selective intersystem crossing, and energy relaxation process. In this diagram, R_1 and R_2 are the doublet ground states of the two dangling radicals. S_0^0, S_1^0, and T_1^0 are the ground and the excited singlet and triplet states of the diphenylanthracene moiety, respectively. The $M_S = \pm 1$ and 0 sublevels of the quintet state are selectively populated by ISC. In the ground state, the singlet state and the triplet state are nearly degenerated and the energy splitting is only $2J_{intra}/k_B = 12$ K (see section 3.2 in the text). The spin state selective decay also occurs from the excited quartet state (Q) to the ground triplet state, which is nearly degenerate to the singlet ground state (see section 3.5 in the text).

between the excited quartet state ($Q_{\pi\pi^*}$) and the dangling doublet radical (R). The spin−orbit wave functions for Qu in eqs 17a−e can be rewritten as follows:

$$|Qu_{\pi\pi^*},+2\rangle = \hat{A}\{|Q_{\pi\pi^*},+3/2\rangle|R\rangle\} \quad (21a)$$

$$|Qu_{\pi\pi^*},+1\rangle = \hat{A}\{(1/2)|Q_{\pi\pi^*},+3/2\rangle|\bar{R}\rangle + (\sqrt{3}/2)|Q_{\pi\pi^*},+1/2\rangle|R\rangle\} \quad (21b)$$

$$|Qu_{\pi\pi^*},0\rangle = \hat{A}\{(1/\sqrt{2})|Q_{\pi\pi^*},+1/2\rangle|\bar{R}\rangle + (1/\sqrt{2})|Q_{\pi\pi^*},-1/2\rangle|R\rangle\} \quad (21c)$$

$$|Qu_{\pi\pi^*},-1\rangle = \hat{A}\{(1/2)|Q_{\pi\pi^*},-3/2\rangle|R\rangle + (\sqrt{3}/2)|Q_{\pi\pi^*},-1/2\rangle|\bar{R}\rangle\} \quad (21d)$$

$$|Qu_{\pi\pi^*},-2\rangle = \hat{A}\{|Q_{\pi\pi^*},-3/2\rangle|R\rangle\} \quad (21e)$$

Here, the operator "$\hat{A}\{...\}$" means an antisymmetric operation with respect to permutation of any pair of electrons. As mentioned, only the $M_S = \pm 1/2$ sublevels of $Q_{\pi\pi^*}$ ($|Q_{\pi\pi^*},\pm 1/2\rangle$) are populated in the selective enhanced ISC mechanism. Therefore, the population of $Q_{\pi\pi^*}$ can be transferred only to the $M_S = \pm 1$ and 0 sublevels of Qu, leading to the selective ISC observed in the quintet TRESR spectrum. The calculated ESP ratios are $P_{0'} = 0.40$, $P_{-1'} = P_{+1'} = 0.30$ and $P_{-2'} = P_{+2'} = 0.0$ and are close in magnitude to the observed ones ($P_{0'} = 0.30$, $P_{-1'} = P_{+1'} = 0.35$ and $P_{-2'} = P_{+2'} = 0.0$), although the calculated $P_{0'}$ is larger. For more satisfactory agreement, the other minor ISC pathways must be taken into account.

3.8. Excited Spin States of the Topological Isomers, 1b and 2b. It is well-known that π-topology plays a very important role in spin alignment in the ground state of the alternant hydrocarbons.[11−15] In the ground state, the spin polarization effect governs the spin alignment and the π-topological rule is well established. The spin multiplicity of the ground state depends drastically on the topology of the π-electron network.[12] To test the role of the π-topology on the spin alignment in the excited state, TRESR experiments were performed for **1b** and **2b**, which are the π-topological isomers of **1a** and **2a**, respectively. In contrast to the result of **1a**, no TRESR signal attributable to the high-spin excited state was observed for **1b** and only a very weak absorptive signal due to the doublet state was observed (Figure 13). The g value for **1b** was $g(D) = 2.001$ (arrow in Figure 13) and is similar to the value ($g = 2.002_0$) estimated from eq 10, indicating that the excited doublet state arises from the radical−excited triplet pair. Although the observed signal shows all characteristics expected for the excited D of **1b**, we cannot completely rule out the overlapping or the possibility of a signal originating from a defect in the quartz insert, which has been observed in the $g \approx 2$ region, because the signal in Figure 13 was obtained as a result of the long accumulation time. In any event, no high-spin TRESR signal for **1b** agrees with the π-topological rule, indicating that the lowest excited state of **1b** is a low-spin doublet ($S = 1/2$) spin state and the sign of the intramolecular exchange is antiferromagnetic. A similar change in the TRESR spectrum was also observed for **2b**, the π-topological isomer of **2a**. No TRESR signal for the excited spin state was observed in **2b**, indicating that the lowest excited state is a low-spin singlet ($S = 0$) spin state, which is ESR silent. Therefore, the intramolecular exchange is antiferromagnetic, similar to that of **1b**. These findings show that the sign of the intramolecular exchange interaction and the spin multiplicity of the lowest excited spin state change drastically depending on the topological nature of the π-electron network. Thus, the π-topological rule of the spin polarization established for the ground states of the aromatic hydrocarbons[11−15] also plays an important role in the spin alignment on the excited states. These findings also indicate the ferromagnetic intramolecular exchange for **1a** and **2a** and the antiferromagnetic one for **1b** and **2b**.

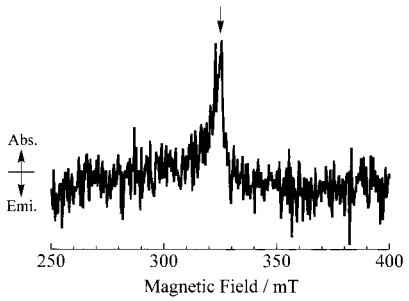

Figure 13. Typical TRESR spectrum of **1b**, which is the π-topological isomer of **1a**. The microwave frequency is 9087.56 MHz. The spectrum was observed in a 2-MTHF rigid glass matrix at 30 K and 1.0 μs after laser excitation by accumulation 400 times.

3.9. Electronic Structures and Mechanism of Spin Alignment on Excited States. To confirm the physical picture of the spin alignment, ab initio molecular orbital calculations based on DFT were performed. The electronic structures of the first excited triplet states (T_1) of the phenylanthracene and diphenylanthracene molecules were calculated using Gaussian 98.[36] The minimum energy structures were determined by a semiempirical molecular orbital calculation (MNDO/AM1 method). In the ab initio calculations, the STO 6-31G basis set and UHF Becke 3LYP hybrid method were employed. Figure 14 shows the one-electron molecular orbital energies of the NHOMO, SOMO, and LUMO and the calculated total spin densities on the carbon sites. In the anthracene moiety of phenyl- or diphenylanthracene molecules, the spin density distributions are

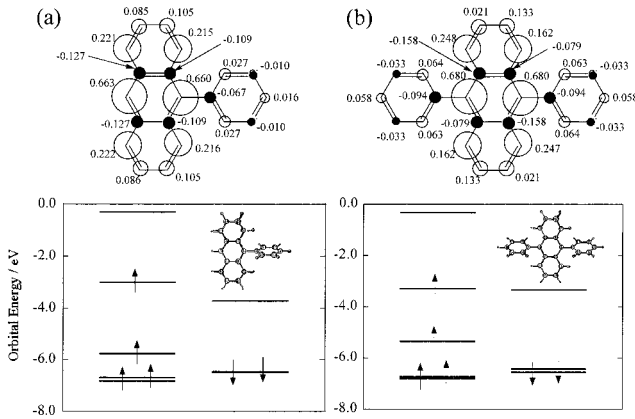

Figure 14. Spin distributions and the location of the UHF one-electron molecular orbitals of the excited triplet states of (a) phenylanthracene and (b) diphenylanthracene. The occupied α- and β-orbitals are shown by the up and down arrows, respectively.

nearly symmetrical (Figure 14). Only the 11, 12, 13, and 14 positions have negative spin densities, and the other carbon sites all have positive spin densities. This spin density distribution shows that spin delocalization overcomes the spin polarization effect on the anthracene moiety. In contrast, the alternating sign of the spin density is realized on the dangling phenyl groups of phenyl- and diphenylanthracenes (Figure 14). This sign alternation of the spin densities shows that the spin polarization mechanism overcomes the spin delocalization within the dangling phenyl groups even in the excited triplet state. The large positive spin densities at the 9 and 10 positions caused by spin delocalization in the anthracene moiety couple with the dangling localized radical spins ($S = 1/2$) through spin polarization of the dangling phenyl groups. This mechanism leads to a ferromagnetic exchange between excited triplet state and radical spins in **1a** and **2a** and to an antiferromagnetic exchange in **1b** and **2b**. The direct overlap between the triplet excited state of the anthracene moiety and the dangling radicals is not dominant in determining the sign of the intramolecular exchange because the closest distance between them is ca. 3.67 Å in **2b**. The long distance leads to a weak interaction compared with that through π-conjugation.[37] The ab initio molecular orbital calculations are consistent with the experimental results and the schematic diagrams of the spin alignment shown in Figures 6 and 8. Therefore, it was concluded that a photoinduced intramolecular ferromagnetic spin alignment occurs for **1a** and **2a**.

4. Conclusions

Direct detection of the excited quartet ($S = 3/2$) and quintet ($S = 2$) states shows that the intramolecular ferromagnetic spin alignment between the doublet spins ($S = 1/2$) in the dangling iminonitroxide radicals and the $\pi\pi^*$ excited triplet state of the phenyl- or diphenylanthracene moiety occurs by photoexcitation. The ferromagnetic spin alignment in the excited state of **2a** indicates that a spin delocalization mechanism is much more dominant for intramolecular spin alignment in the excited state than in the ground state. The unpaired spin in the iminonitroxide group is coupled to the phenyl- or diphenylanthracene moiety through π-conjugation according to the π-topological rule for the spin polarization.[11−15] The observation of Qu in **2a** and theoretical calculations show that spin delocalization overcomes spin polarization in the excited triplet state of the diphenylanthracene spin coupler, giving the same sign of the spin densities at the 9 and 10 positions of the anthracene moiety. As a result, all the unpaired spins are aligned parallel in the photoexcited state of **2a**, giving Qu detected by the TRESR experiments. Since a weak antiferromagnetic exchange interaction was observed in the ground state of this system, the effective exchange coupling between the two dangling radicals through the diphenylanthracene spin coupler changed from antiferromagnetic to ferromagnetic by photoexcitation (Figure 8). This phenomenon originates from the results that the photoexcited triplet state of the anthracene moiety couples ferromagnetically to the radical spins and the coupling is larger than the direct interactions between the two dangling radical spins. Thus, photoinduced spin alignment and sign inversion of the effective exchange coupling utilizing the excited triplet molecular field were achieved for the first time on a purely organic π-conjugated system. In contrast to **1a** and **2a**, no such high-spin excited state was detected for their topological isomers, **1b** and **2b**, under the same experimental conditions. This result clearly shows that the drastic change in the spin states occurs in the excited state, depending on the topological nature of the π-electron network. Although the importance of the π-topology is well established for the spin alignment in the ground state, it has not been tested for the excited state. This work is the first systematic study on the role of the π-topology in the photoexcited state, and TRESR experiments for the π-conjugated spin systems have clearly demonstrated the importance of the π-topology in the spin alignment of the excited states.

Acknowledgment. We thank Professor Seigo Yamauchi (Tohoku University) and Professor Toshio Matsushita (Osaka City University) for their helpful discussions. We also thank Mr. Koji Iimura for his earlier assistance in the set up of our TRESR apparatus and Dr. B. K. Breedlove for a careful reading of our final manuscript and for kind suggestions about wording. This work was financially supported by PRESTO from the Japan Science and Technology Corp.

JA001920K

(36) The DFT calculation was carried out using Gaussian 98, Revision A.7: Frisch, M. J.; Trucks, G. W.; Schlegel, H. B.; Scuseria, G. E.; Robb, M. A.; Cheeseman, J. R.; Zakrzewski, V. G.; Montgomery, J. A., Jr.; Stratmann, R. E.; Burant, J. C.; Dapprich, S.; Millam, J. M.; Daniels, A. D.; Kudin, K. N.; Strain, M. C.; Farkas, O.; Tomasi, J.; Barone, V.; Cossi, M.; Cammi, R.; Mennucci, B.; Pomelli, C.; Adamo, C.; Clifford, S.; Ochterski, J.; Petersson, G. A.; Ayala, P. Y.; Cui, Q.; Morokuma, K.; Malick, D. K.; Rabuck, A. D.; Raghavachari, K.; Foresman, J. B.; Cioslowski, J.; Ortiz, J. V.; Baboul, A. G.; Stefanov, B. B.; Liu, G.; Liashenko, A.; Piskorz, P.; Komaromi, I.; Gomperts, R.; Martin, R. L.; Fox, D. J.; Keith, T.; Al-Laham, M. A.; Peng, C. Y.; Nanayakkara, A.; Gonzalez, C.; Challacombe, M.; Gill, P. M. W.; Johnson, B.; Chen, W.; Wong, M. W.; Andres, J. L.; Gonzalez, C.; Head-Gordon, M.; Replogle, E. S.; Pople, J. A., Gaussian, Inc., Pittsburgh, PA, 1998.

(37) The iminonitroxide radical couples with the anthracene moiety through a π-conjugated spin polarization on the dangling phenyl group. The magnitude of J was estimated by the following equation: $J_{\mathrm{eff}} \approx J_{\mathrm{coupler}}\rho(i)\,\rho(j)/4S_{\mathrm{A}}S_{\mathrm{B}}$. $\rho(i)$ and $\rho(j)$ are the spin densities at the connecting positions of the triplet anthracene derivative and the iminonitroxide radical. J_{coupler} is the effective exchange of the phenyl coupler and is estimated to be larger than 2000 cm^{-1}. (See: Ishida, T.; Iwamura, H. *J. Am. Chem. Soc.* **1991**, *113*, 4238. In this paper, the magnetic exchange was determined to be 500 K for *m*-phenylenebis(nitroxide).) In **2b**, the spin densities were estimated to be ca. 0.68 at the 9 and 10 positions of the triplet anthracene (see Figure 14b) and ca. 0.09 at the linking position of the iminonitroxide radical (not shown in this paper). The spin densities were obtained by the ab initio MO calculations. $J_{\mathrm{eff}}(\pi-\pi)$ through π-conjugation was estimated to be ca. 60 cm^{-1}, when the moieties were coplanar. Actually, $J_{\mathrm{eff}}(\pi-\pi)$ will be 10−30 cm^{-1} for **2b** as a result of the torsion angle. The maximum exchange through the direct overlap was estimated using $(1/4S_{\mathrm{A}}S_{\mathrm{B}})(4t^2/U)\,\rho(\mathrm{C})\,\rho(\mathrm{O})\cos^2\theta$ and $t = -\beta_{\mathrm{C-N}}\exp(-d/1.45)$. $\rho(\mathrm{C})$ and $\rho(\mathrm{O})$ are the spin densities at the overlapping carbon position ($\rho(\mathrm{C}) = 0.25$; see Figure 14b) of the triplet anthracene derivative and at the oxygen atom ($\rho(\mathrm{O}) = 0.50$) of the iminonitroxide radical. Using $U \approx 10$ eV and $\beta_{\mathrm{C-N}} \approx 1.5$ eV, J_{eff} due to the direct overlap was estimated to be smaller than 3 cm^{-1} (∼2.5 cm^{-1} for $\cos^2\theta = 1$) for **2b**.

(38) Teki, Y. Takui, T., Itoh, K. *J. Chem. Phys.* **1988**, *88*, 6134.